Journal of Nano- and Electronic Physics
Vol. **18** No 3, 03032(7pp) (2026)

Журнал нано- та електронної фізики
Том **18** № 3, 03032(7cc) (2026)

OPEN ACCESS

REGULAR ARTICLE

Structural and Optical Study of Er_2O_3 Thin Films Grown by Spray Pyrolysis from Erbium Nitrate

O.V. Moskalenko[1,*], A.B. Liapina[2,†], O.M. Strilchuk[2], L.V. Shcherbyna[2], T.V. Torchynska[3]

[1] *Mykola Gogol State University of Nizhyn, 16600 Nizhyn, Ukraine*
[2] *V. Lashkaryov Institute of Semiconductor Physics, NAS of Ukraine, 03028 Kyiv, Ukraine*
[3] *Instituto Politécnico Nacional, ESFM, 07738 México City, Mexico*

(Received 15 January 2026; revised manuscript received 16 June 2026; published online 26 June 2026)

This paper reports on the relationship between the crystalline structure and optical properties of Er_2O_3 films grown by spray pyrolysis. The films were deposited on Si(100) substrates heated to 400 °C via thermal decomposition of an erbium nitrate precursor. Additional annealing was performed at 600 and 800 °C in a nitrogen atmosphere. The structural and optical properties of the films were investigated in comparison with powder samples using X-ray diffraction (XRD), Raman spectroscopy, and Fourier transform infrared (FTIR) spectroscopy, complemented by an analysis of precursor decomposition. XRD results confirm the formation of single-phase cubic Er_2O_3 with a bixbyite structure. A pronounced preferred crystallographic orientation is observed in thin films, in contrast to randomly oriented powder samples. Annealing significantly enhances diffraction peak intensity without noticeable changes in peak positions, indicating improved crystallinity and texture development without phase transformation. Raman spectra reveal a gradual evolution from a disordered structure in as-deposited films to well-defined vibrational modes associated with Er–O bonds after annealing. FTIR analysis confirms the formation of Er–O bonds and the absence of nitrate-related features, indicating complete precursor decomposition. The results demonstrate that thermal treatment plays a crucial role in transforming precursor-derived films into chemically pure and structurally ordered Er_2O_3 with pronounced preferred orientation governed by substrate effects and growth conditions.

Keywords: Erbium oxide, Thin films, XRD, FTIR, Raman scattering.

DOI: 10.21272/jnep.18(3).03032 PACS numbers: 61.66.Fn, 68.55. – a, 78.30. – j, 82.30.Lp

1. INTRODUCTION

Rare-earth oxide thin films attract considerable attention due to their potential applications in nano- and electronic devices, including high-k dielectrics, optical coatings, and integrated photonic structures. Among them, erbium oxide (Er_2O_3) is of particular interest owing to its relatively high dielectric constant ($k \approx$ 10-20) [1], wide band gap (~ 5.5-6.5 eV) [2, 3], and optical activity of Er^{3+} ions associated with intra-4f electronic transitions [1, 5]. These properties make Er_2O_3 a promising material for dielectric and optoelectronic applications.

Various techniques have been developed for the deposition of Er_2O_3 thin films, including vapor-phase methods such as metal-organic CVD [1, 5], aerosol assisted CVD [6], atomic layer deposition (ALD) [3, 7]), as well as solution-based approaches, including sol-gel [8, 9], spin-coating [1] and spray-pyrolysis [11, 12]. Among these, spray pyrolysis is considered as a simple and cost-effective technique suitable for large-area deposition, where film formation occurs through thermal decomposition of precursor droplets on a heated substrate.

In such processes, the properties of the precursor play a decisive role in determining the film formation mechanism, phase composition, and defect structure. In particular, suitable precursors must exhibit sufficient solubility, chemical stability in solution, and controlled thermal decomposition leading to oxide formation. Various classes of erbium precursors have been reported, including inorganic salts and metal-organic compounds, which differ significantly in their solubility and decomposition behavior.

Inorganic lanthanide nitrate precursors show high solubility in polar solvents such as water and ethanol [13, 14], making them well suited for spray-based techniques. However, they undergo multistep thermal decomposition involving the formation of intermediate species. In contrast, metal-organic precursors $Er(TMHD)_3$ and $Er(CpMe)_3$ may exhibit more controlled decomposition behavior [4, 7, 15], but their limited solubility and reduced stability complicate their use in solution-based deposition. Unlike these organometallic precursors, erbium nitrate, $Er(NO_3)_3{\cdot}xH_2O$, represents a a relatively stable and safer compound that can be easily processed in polar solvents.

* Correspondence e-mail: mov5@ukr.net
† a_lyapina@i.ua

Cite this article as: O.V. Moskalenko et al., *J. Nano- Electron. Phys.* 18 No 3, 03032 (2026) https://doi.org/10.21272/jnep.18(1).03032

Based on these considerations, erbium nitrate was selected in this work as a model precursor, and spray pyrolysis was employed for thin film deposition. The structural and optical properties of the resulting Er_2O_3 thin films were investigated using Raman spectroscopy, X-ray diffraction (XRD), and Fourier transform infrared (FTIR) spectroscopy. The results provide insight into the relationship between crystalline structure, local bonding, and electronic properties, which is essential for the optimization of Er_2O_3-based materials for nano- and electronic applications.

2. EXPERIMENTAL DETAILS

Er_2O_3 thin films were deposited by a spray pyrolysis technique using a home-built setup operating at atmospheric pressure. Single-crystalline silicon substrates with (100) orientation, 2 inches in diameter and a resistivity of 15 Ω·cm, were used for film growth. Prior to deposition, the substrates were sequentially cleaned in acetone and ethanol, rinsed in deionized water, and dried in air.

The precursor solution was prepared using erbium nitrate hydrate ($Er(NO_3)_3{\cdot}6H_2O$, analytical grade, Alfa Aesar) dissolved in the mixture of distilled water and ethanol (1:1 by volume) under magnetic stirring at room temperature. The precursor concentration was adjusted to 0.05 M. The resulting solution was filtered to remove possible insoluble particles and continuously stirred during deposition. The solution was atomized using compressed air and sprayed onto the heated substrate through a nozzle positioned at a distance of approximately 10-12 cm. The flow rate was maintained at approximately 1-2 ml/min. Under these conditions, the film growth rate was estimated to be about 8-10 nm/min. The deposition time (number of spray pulses) was adjusted to obtain films with a thickness of approximately 180 nm.

The deposition was carried out in a pulsed spray regime in order to allow sufficient time for solvent evaporation and precursor decomposition between successive spray cycles. This approach prevents excessive cooling of the substrate and ensures uniform film formation.

The film formation mechanism is governed by the thermal decomposition of erbium nitrate during droplet evaporation and subsequent pyrolytic conversion on the heated substrate. The thermal decomposition behavior of $Er(NO_3)_3{\cdot}6H_2O$ was previously analyzed using a stepwise heating approach. The main decomposition stages are summarized in Appendix A. The results reveal a multistage decomposition process involving dehydration, formation of intermediate oxynitrate species, and final conversion to Er_2O_3 similar to the results reported in [16-18].

During film deposition, the substrates were placed on a heated plate and maintained at temperatures in the range of 400 °C. The spray process was carried out in a pulsed regime, allowing sufficient time between spray cycles for solvent evaporation and precursor decomposition, thus preventing excessive cooling of the substrate and ensuring uniform film growth.

After deposition, the samples were allowed to cool naturally to room temperature under ambient conditions. The coated substrates were then cut into square pieces with dimensions of approximately 1×1 cm^2 for further characterization.

Additional, post-deposition annealing was performed at temperatures of 600 and 800 °C for 10 min in a nitrogen atmosphere to get insight on the evolution of structural and optical properties of the films.

Structural characterization was carried out using Raman spectroscopy and X-ray diffraction (XRD) methods. Raman spectra were recorded with a 785 nm excitation source (StellarNet Inc., USA) with a spectral resolution of approximately 4 cm^{-1}. The laser power was kept sufficiently low to avoid thermal or structural modification of the samples. XRD measurements were performed using a Philips X'Pert-MRD diffractometer with Cu Kα radiation ($\lambda = 0.15406$ nm) in grazing-incidence (ω–2θ) geometry. Phase identification was carried out using the Powder Diffraction File (PDF) database (card No. 01-074-1983). FTIR transmission spectra were measured using a Shimadzu IRTracer-100 spectrophotometer with a spectral resolution of 1 cm^{-1} at room temperature.

3. RESULTS AND DISCUSSION

3.1 XRD Data

Figure 1 shows the XRD patterns of Er_2O_3 films, as-deposited (curve 1) and those annealed at 600 °C (curve 2) and 800 °C (curve 3). For comparison, the XRD pattern of a powder sample prepared from the same precursor is shown by curve 4. The diffraction pattern of the powder sample exhibits peak positions and relative intensities consistent with cubic Er_2O_3 (bixbyite structure), indicating the formation of a randomly oriented polycrystalline material. The most intense reflection corresponds to the (222) plane, which is characteristic of Er_2O_3 powders.

The XRD pattern of as-deposited film (curve 1) reveals diffraction peaks located at approximately 2θ = 29.4°, 34.3°, 44.5°, 49.1°, 52.6°, and 58.2°, which can be attributed to the (222), (400), (431)/(332), (440), (611) and (622) planes, respectively. These peaks match well the reference pattern of cubic Er_2O_3. The lattice parameter, calculated from the XRD data, is approximately $a \approx 10.55$ Å, which is in good agreement with the standard value ($a = 10.548$ Å). This indicates that no significant lattice distortion is present. However, the relative intensities of the diffraction peaks differ significantly from those of a randomly oriented powder sample (Fig. 1). In particular, the reflections (400) and (431)/(332) exhibit significantly higher intensity compared to the (222) peak (curve 1). The intensity ratio I(222)/I(400) decreases from approximately 3.0 in the powder sample to about 0.44 in the film. This indicates the presence of a preferred crystallographic orientation (texture) in the film similar to the results reported in [10, 19, 20] that is likely influenced by the Si(100) substrate and the growth conditions during deposition.

A slight shift of the XRD peaks compared to powder sample and standard reference positions may be attributed to residual stresses in the film. Such stresses can arise from lattice mismatch between the film and the Si substrate, as well as from thermal expansion differences during cooling after deposition.

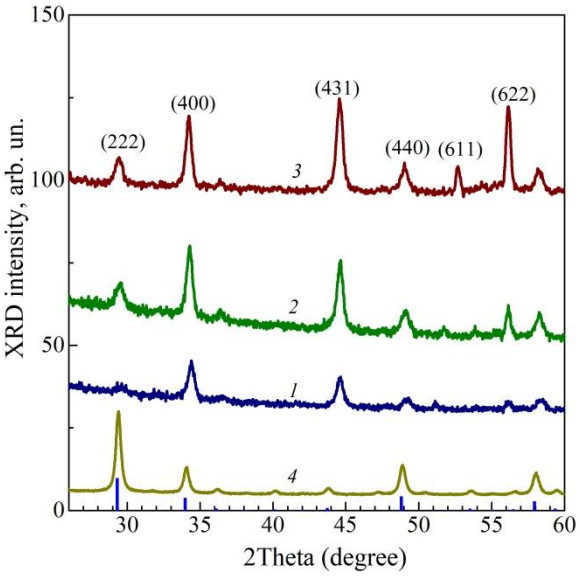

Fig. 1 – XRD patterns for the Er_2O_3 films: as-deposited (400 °C) (1) and annealed at T = 600 (2) and 800 °C (3). Curve 4 corresponds to Er_2O_3 commercial powder with cubic structure shown for comparison

The XRD pattern of the annealed thin films shows a significant redistribution of peak intensities while preserving the same set of diffraction peaks. The reflections observed at $2\theta \approx 29.5°$, 34.3°, 44.5°, 49.1°, 52.6°, and 56-58° can be indexed to the (222), (400), (431)/(332), (440), (611), and (622) planes of cubic Er_2O_3, confirming the formation of a single-phase oxide. However, the relative intensities differ markedly from those of the powder and as-deposited sample. In particular, the (222) reflection is strongly suppressed in the annealed films, while the (400), (431), and (622) reflections are significantly enhanced. The intensity ratio I(222)/I(400) continue to decrease for annealed films to about 0.35 in the film annealed at 800 °C, clearly indicating the presence of preferred crystallographic orientation (texture).

Such behavior suggests that the crystallographic growth of Er_2O_3 in thin-film form is not random but governed by substrate-induced effects and growth conditions during spray pyrolysis and subsequent annealing. The Si(100) substrate likely influences nucleation and growth, leading to anisotropic development of crystallites and preferred alignment of specific crystallographic planes.

In addition to intensity redistribution, a slight shift of diffraction peaks relative to standard reference positions is observed. Most reflections are shifted toward higher 2θ values, indicating the presence of compressive strain within the film. The estimated strain is on the order of 10^{-2}, which is typical for oxide thin films deposited on silicon substrates [10, 19]. The variation of peak shifts among different reflections suggests anisotropic strain, associated with the textured structure and relaxation processes during annealing.

No additional peaks corresponding to secondary phases or monoclinic Er_2O_3 were detected, indicating that the films are predominantly single-phase cubic Er_2O_3. Minor weak features may be attributed to structural disorder or low-intensity contributions from less favorable crystallographic orientations.

Overall, the XRD analysis demonstrates that the films consist of a textured cubic Er_2O_3 phase with significant preferential orientation and residual strain, resulting from the combined effects of substrate interaction, deposition conditions, and post-deposition thermal treatment.

3.2 Raman Scattering Spectra

Figure 2 shows Raman spectra of the same as-deposited and annealed Er_2O_3 films (curves 1-3), together with spectra of the powder reference sample (curve 4) and the Si substrate (curve 5). The powder sample exhibits a well-defined Raman bands in the range of 100-700 cm^{-1} (~ 115 cm^{-1} (A_g), ~ 227 cm^{-1}, ~ 260 cm^{-1} ($F_g + E_g$), ~ 375 cm^{-1} (F_g), ~ 483 cm^{-1} (F_g), and ~ 590-600 cm^{-1} (F_g)), which can be attributed to lattice vibrations and Er–O stretching modes characteristic of cubic Er_2O_3 [21, 22].

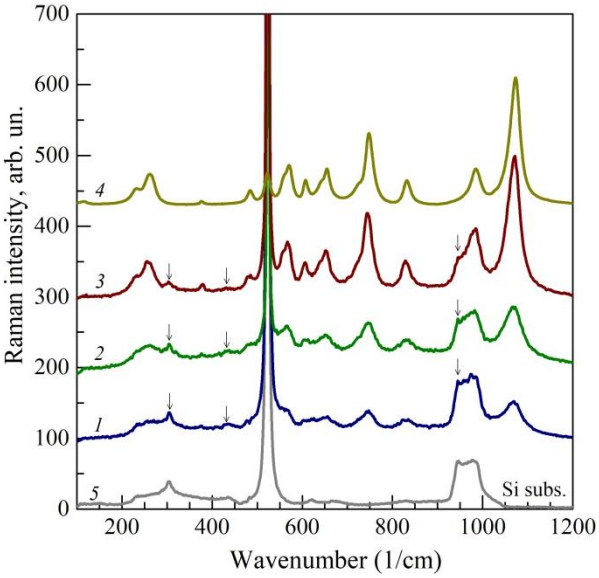

Fig. 2 – Raman scattering spectra for the Er_2O_3 films: as-deposited (400 °C) (1) and annealed at T = 600 (2) and 800 °C (3). Curve 4 corresponds to Er_2O_3 commercial powder with cubic structure shown for comparison, curve 5 demonstrate signal from Si substrate to reveal its contribution in the spectra of the films near 520.6 cm^{-1}. Arrows near curved 1-3 show the signal from Si substrate

Additional features observed at higher wavenumbers (> 700 cm^{-1}) cannot be directly assigned to first-order Raman modes of Er_2O_3. These signals are likely associated with multiphonon processes and/or luminescence contributions related to Er^{3+} ions. The presence of high-wavenumber features reflects the complex interplay between vibrational and electronic processes in rare-earth oxide system. A strong narrow band at approximately 520 cm^{-1} originates from the Si substrate and partially overlaps with the film signal, which must be taken into account in the spectral analysis.

The as-deposited film shows significantly main Raman bands at ~ 260 cm^{-1} ($F_g + E_g$) and ~ 590-600 cm^{-1} (F_g)) (Fig. 2, curve 2). These bands are broader, poorly resolved, and less intense, indicating some structural disordering in the Er–O network.

After annealing at 600 °C, the Raman spectrum exhibits a noticeable increase in peak intensity and partial narrowing of the bands mentioned above, reflecting the onset of improved short-range order. Further annealing at 800 °C leads to well-defined and sharper Raman peaks whose positions and relative intensities approach those of the powder sample. The positions of the main Raman bands in 100-600 cm^{-1} range remain essentially unchanged after annealing, indicating that the same crystalline phase is preserved. However, the progressive increase in peak intensity and reduction in bandwidth clearly demonstrate improved crystallinity and structural ordering in the films.

For all films, the bands observed at higher wavenumbers (> 700 cm^{-1}) are attributed to multiphonon processes and possible luminescence contributions associated with Er^{3+} ions. The presence of these features in both powder and film spectra confirms their intrinsic origin related to Er_2O_3, whereas the evolution of Raman spectra with annealing temperature reveals the formation of well-ordered cubic Er_2O_3 structure and supports XRD findings.

It should be pointed out that no Raman features corresponding to nitrate groups [13, 23] were observed, indicating complete decomposition of the precursor and formation of oxide phase. This statement is further confirmed by FTIR spectra recorded for the same samples.

3.3 FTIR Spectroscopy

Figure 3 shows FTIR transmission spectra of the as-deposited Er_2O_3 films (curve 1) and films annealed at 600 °C (curve 2) and 800 °C (curve 3). The spectrum of the silicon substrate is also presented for comparison (curve 4). The as-deposited film exhibits a broad absorption band in the 250-600 cm^{-1} region, where several distinguishable peaks are observed at approximately 285, 332, 366, and 560 cm^{-1}. These features are attributed to Er–O vibrational modes, including lattice vibrations and stretching modes. The presence of these resolved peaks indicates the formation of an erbium–oxygen network

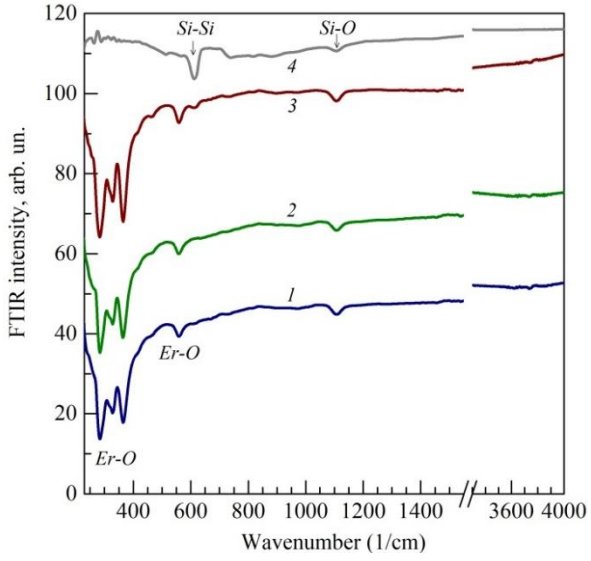

Fig. 3 – FTIR transmission spectra for the Er_2O_3 films: as-deposited (400 °C) (1) and annealed at T = 600 (2) and 800 °C (3). Curve 4 shows the FTIR spectrum from Si substrate

already in the as-deposited film, suggesting the onset of structural ordering. A distinct absorption band near ~ 1110 cm^{-1} is observed and can be attributed to the Si substrate, as confirmed by the reference spectrum (curve 4).

No absorption bands related to nitrate groups are detected in the 1300-1500 cm^{-1} region, indicating effective decomposition of the precursor (Fig. 3). In addition, no noticeable absorption features are observed in the 3200-3700 cm^{-1} range, suggesting the absence of hydroxyl groups or residual water in the films.

Upon annealing at 600 °C and 800 °C, the FTIR spectra show a slight sharpening of the bands in the 250-600 cm^{-1} range, while their positions remain nearly unchanged. This behavior indicates that annealing improves structural ordering and local bonding environment without altering the phase composition.

For the film annealed at 800 °C, an additional feature appears near ~ 610 cm^{-1} while the band near 1110 cm^{-1} increases in intensity (Fig. 3, curve 3). Both these bands correspond to characteristic vibration in the Si substrate (curve 4). This effect can be explained by an increase in film transparency upon annealing, allowing greater contribution of the substrate signal to the measured spectrum. Alternatively, this feature may also reflect improved densification and reduction of scattering losses in the film, which enhances transmission and reveals otherwise weaker substrate-related modes.

Overall, the FTIR results confirm the complete decomposition of Er nitrate upon film deposition and the formation of Er–O bonds' network. Besides improved structural ordering, optical transparency of the films increases, while maintaining the same chemical composition.

4. DISCUSSION

The analysis of the results obtained from XRD, Raman scattering, and FTIR studies provide a consistent picture of the structural evolution of Er_2O_3 films during deposition and subsequent annealing.

The decomposition behavior of the erbium nitrate precursor suggests that film formation occurs under non-equilibrium conditions during spray pyrolysis. Although stepwise thermal analysis of Er nitrate decomposition indicates a multistep decomposition pathway involving intermediate nitrate and oxynitrate species, such intermediates are not observed in the films. This can be explained by rapid solvent evaporation and fast thermal decomposition upon droplet impact on the heated substrate, leading directly to the formation of an Er–O network.

FTIR and Raman data confirm the absence of nitrate-related features, indicating complete precursor decomposition already at the deposition stage. This demonstrates that spray pyrolysis provides sufficiently high local temperatures to achieve effective oxide formation even at relatively moderate substrate temperatures.

XRD and Raman results show that annealing does not induce phase transformation, as the cubic Er_2O_3 structure is preserved. Instead, thermal treatment enhances crystallinity, as evidenced by increased peak intensity in XRD patterns and sharpening of Raman bands. This indicates that structural ordering occurs

primarily during post-deposition annealing through grain growth and relaxation processes.

The strong preferred orientation observed in thin films, which is absent in powder samples, suggests that crystallite growth is governed by substrate-induced effects. The Si(100) substrate influences nucleation and growth, leading to anisotropic development of crystallographic planes and formation of texture similar to the results reported in [10]. The presence of residual strain detected by XRD peak shifts further supports the role of lattice mismatch and thermal stresses in determining film structure.

The appearance of substrate-related features in FTIR spectra after annealing is attributed to improved film transparency and densification, which reduce scattering and reveal weak substrate signals. At the same time, no formation of Er silicate phases testifies to the stability of the films in direct contact with Si substrate upon annealing that opens the way for the microelectronic application.

Thus, the results reported above show that the formation of the Er_2O_3 films and their structural evolution are controlled by the interplay between precursor decomposition kinetics, substrate effects, and thermal treatment conditions.

5. CONCLUSIONS

Er_2O_3 thin films were successfully deposited on Si(100) substrates by spray pyrolysis using an erbium nitrate precursor. Structural and spectroscopic analyses confirm the formation of single-phase cubic Er_2O_3. It is shown that the precursor undergoes rapid decomposition during deposition, leading to the formation of an Er–O network without detectable nitrate residues; the films exhibit pronounced preferred crystallographic orientation induced by the substrate; annealing at 600 °C and 800 °C does not change the cubic phase but improves crystallinity and structural ordering. Raman and FTIR data confirm the formation of Er–O bonds and the absence of residual precursor-related species. The results demonstrate that control of precursor chemistry, deposition conditions, and thermal treatment enables the fabrication of chemically pure and structurally ordered Er_2O_3 thin films with tailored crystallographic orientation.

REFERENCES

1. K.H. Goh, A.S.M.A. Haseeb, Y.H. Wong, *Mater. Sci. Semicond. Proc.* **68**, 302 (2017) https://doi.org/10.1016/j.mssp.2017.06.037.
2. C. Liu, A. Wei, Y. Liu, *Acta Opt. Sin.* **29**, 1724 (2009).
3. T. Ji, L. Peng, Z. Fang, Y. Cui, Y. Hao, *Appl. Phys. A* **115**, 797 (2014) https://doi.org/10.1007/s00339-013-7870-5.
4. L. Khomenkova, H. Merabet, M.-P. Chauvat, C. Frilay, X. Portier, C. Labbe, P. Marie, J. Cardin, S. Boudin, J.-M. Rueff, F. Gourbilleau, *Surf. Interfaces* **34**, 102377 (2022) https://doi.org/10.1016/j.surfin.2022.102377.
5. Y. Hishinuma, T. Tanaka, T. Tanaka, T. Nagasaka, Y. Tasaki, A. Sagara, T. Muroga, *Fusion Engineering and Design* **86**, 2530 (2011) https://doi.org/10.1016/j.fusengdes.2011.04.043.
6. J. Borowiec, C.J. Carmalt, M.O. Blunt, I.P. Parkin, *Colloid. Surfaces A: Physicochem. Eng. Aspect.* **707**, 135912 (2024) https://doi.org/10.1016/j.colsurfa.2024.135912.
7. J. Päiväsaari, J. Niinistö, K. Arstila, K. Kukli, M. Putkonen, L. Niinistö, *Chem. Vapor Depos.* **11**, 415 (2005) https://doi.org/10.1002/cvde.200506396.
8. G. Wang, D. Liu, S. Fan, Z. Li, J. Su, *Nanotechnology* **32**, 215202 (2021) https://doi.org/10.1088/1361-6528/abe439
9. A. Abdullah, E.M. Benchafia, D. Choi, S. Abedrabbo, *Nanomaterials* **13**, 1508 (2023) https://doi.org/10.3390/nano13091508.
10. M.M. Giangregorio, A. Sacchetti, M. Losurdo, P. Capezzuto, G. Bruno, *J. Non-Cryst. Solids* **354**, 5254 (2008) https://doi.org/10.1016/j.jnoncrysol.2007.10.102.
11. D. Perednis, L.J. Gauckler, *J. Electroceram.* **14**, 103 (2005).
12. O.J. Ilegbusi, S.M.N. Khatami, L.I. Trakhtenberg, *Mater. Sci. Appl.* **8**, 153 (2017).
13. B.V. Ayodele, M.A. Hossain, S.L. Chong, J.C. Soh, S. Abdullah, M.R. Khan, C.K. Cheng, *J. Therm. Anal. Calorim.* **125**, 423 (2016) https://doi.org/10.1007/s10973-016-5450-6.
14. V. Lozovan, L.E. Mureşan, I. Perhaiţa, G. Borodi, A.-I. Cadis, I. Bulhac, O. Danilescu, M. Muresan-Pop, A. Turza, *Inorganica Chimica Acta* **598**, 123177 (2026) https://doi.org/10.1016/j.ica.2026.123177.
15. J.K. Patel, I. Ramzan, C.I. De Leon Reyes, I.P. Parkin, C.J. Carmalt, *Langmuir* **41**, 15562 (2025) https://doi.org/10.1021/acs.langmuir.5c01723.
16. G.A.H. Mekhemer, B.A.A. Balboul, *Colloid. Surfaces* **181**, 19 (2001). https://doi.org/10.1016/s0927-7757(00)00731-7.
17. A. Bregman, J. Rimsza, M. Ringgold, N. Bell, L. Treadwell, *SN Appl. Sci.* **3**, 341 (2021) https://doi.org/10.1007/s42452-021-04288-y.
18. G.A.M. Hussein, D.J. Buttrey, P. DeSanto, A.A. Abd-Elgaber, H. Roshdy, A.Y.Z. Myhoub, *Thermochimica Acta* **402**, 27 (2002) https://doi.org/10.1016/s0040-6031(02)00535-x.
19. M.M. Giangregorio, M. Losurdo, A. Sacchetti, P. Capezzuto, G. Bruno, G. Malandrino, I.L. Fragalà, R. Lo Nigro, L. Armelao, D. Barreca, E. Tondello, *Appl. Phys. Lett.* **91**, 061923 (2007) https://doi.org/10.1063/1.2768915
20. Y.-H. Chang, M.-H. Chou, T.-J. Wang, *Ceram. Intern.* **44**, 1163 (2017) https://doi.org/10.1016/j.ceramint.2017.10.099.
21. D.S. Knight, W.B. White, *Spectrochimica Acta A* **46**, 381 (1990) https://doi.org/10.1016/0584-8539(90)80109-c.
22. Raman M.V. Abrashev, N.D. Todorov, J. Geshev, *J. Appl. Phys.* **116**, 103508 (2014) https://doi.org/10.1063/1.4894775.
23. G.A.M. Hussein, B.C. Gates, *J. Catal.* **176**, 395 (1998) https://doi.org/10.1006/jcat.1998.2067.

APPENDIX A

A.1. Analysis of Thermal Decomposition of Erbium Nitrate

The thermal decomposition behavior of erbium nitrate hydrate, $Er(NO_3)_3{\cdot}6H_2O$, was analyzed in laboratory using a stepwise heating approach combined with mass measurements.

In the initial stage (Step I, T = 50-120 °C), a gradual mass loss is observed, corresponding to the removal of physically adsorbed water and the onset of stepwise

dehydration (Table 1). This behavior is consistent with the results reported in Ref. [13] for rare-earth nitrates.

At the step II, T = 170-240 °C, a more pronounced mass loss is observed, which is attributed to the complete dehydration and the formation of anhydrous erbium nitrate, $Er(NO_3)_3$. This anhydrous phase is thermally unstable and exists only within a narrow temperature range before further decomposition [16,17].

Further heating up to T = 310-340° C (step III) leads to Er nitrate decomposition through the formation of oxynitrate species, generally described as Er–O–NO_3 compounds. This stage is associated with the release of nitrogen-containing gaseous products and reflects the gradual transformation of the precursor.

At step IV, T = 350-450 °C, complete decomposition of nitrate groups occurs, resulting in the formation of erbium oxide occurs. Above this temperature (step V), the mass stabilizes, indicating the formation of thermally stable Er_2O_3.

Table A1 – Decomposition stages of $Er(NO_3)^3 \cdot 6H_2O$ derived from stepwise thermal analysis

Step	Temperature (°C)	Mass loss (%)	Process
I	50-120	~ 4	Removal of adsorbed water and initial dehydration $Er(NO_3)_3 \cdot 6H_2O \rightarrow Er(NO_3)_3 \cdot xH_2O$
II	170-240	~ 20	Complete dehydration and formation of unstable anhydrous nitrate $Er(NO_3)_3 \cdot H_2O \rightarrow Er(NO_3)_3$
III	310-340	~ 25	Formation of intermediate oxynitrate species $Er(NO_3)_3 \rightarrow ErO_x(NO_3)_y$
IV	350-450	~ 30-57	Decomposition of nitrate groups and formation of erbium oxide $ErO_x(NO_3)_y \rightarrow Er_2O_3$
V	> 450	~ constant	Formation of thermally stable Er_2O_3 phase

The obtained results reveal a multistage mass loss process typical for rare-earth nitrate precursors and consistent with previously reported data for other lanthanide nitrates [16, 17, 18]. This confirms that the decomposition of erbium nitrate follows the general behavior characteristic of lanthanide, including stepwise dehydration, formation of intermediate oxynitrate species, and final conversion to the oxide phase.

These data provide a general understanding of the decomposition pathway, whereas the actual film formation process is governed by dynamic conditions at the heated substrate. While the decomposition of erbium nitrate proceeds through multiple intermediate stages under gradual heating, the conditions during spray pyrolysis are characterized by rapid solvent evaporation and non-equilibrium thermal processes. As a result, decomposition may occur more rapidly and lead directly to the formation of Er_2O_3 during film growth. It should be noted that the substrate temperature used for spray pyrolysis deposition (400 °C) differs from the temperature ranges obtained from stepwise thermal analysis under near-equilibrium conditions.

DECLARATION OF COMPETING INTEREST

The authors declare that they have no known competing financial interests or personal relationships that could have appeared to influence the work reported in this paper.

ACKNOWLEDGEMENTS

The research was partially supported by the National Academy of Sciences of Ukraine.

DATA AVAILABILITY

Data will be made available on request.

AUTHORSHIP CONTRIBUTION STATEMENT

Moskalenko O.V.: Writing – original draft, Writing – review & editing, Investigation, Formal analysis; **Liapina A.B.:** Investigation, Visualization; Writing – review & editing; **Strilchuk O.M.:** Investigation, Formal analysis, Writing – review & editing; **Shcherbyna L.V.:** Investigation; Writing – review & editing; **Torchynska T.V.**: Validation; Writing – review & editing.

Дослідження структурних та оптичних властивостей тонких плівок Er_2O_3, вирощених методом спрей-піролізу з нітрату ербію

О.В. Москаленко[1], А.Б. Ляпіна[2], О.М. Стрільчук[2], Л.В. Щербина[2], Т.В. Торчинська[3]

[1] *Ніжинський державний університет імені Миколи Гоголя, 16600 Ніжин, Україна*
[2] *Інститут фізики напівпровідників ім. В.Є. Лашкарьова, НАН України, 03028 Київ, Україна*
[3] *Національний політехнічний інститут, ВШФМ, 07738 Мехіко, Мексика*

У цій роботі досліджено взаємозв'язок між кристалічною структурою та оптичними властивостями плівок Er_2O_3, отриманих з нітрату ербію методом спрей-піролізу. Проаналізовано процесу термічного розкладу нітрату ербію та визначено умови осадження плівок. Плівки Er_2O_3 було нанесено на пластини Si(100), нагрітої до 400 °C. Додаткові відпали проводилися при 600 °C та 800 °C в атмосфері азоту. Структурні й оптичні властивості плівок досліджували за допомогою дифракції рентгенівських променів, спектроскопії комбінаційного розсіяння світла та інфрачервоної спектроскопії у порівнянні з еталонними порошками. Результати рентгенівської дифракції підтверджують формування плівок з кубічною структурою біксбіту та текстурою на відміну від порошкових зразків із випадковою орієнтацією зерен. Додатковий відпал сприяє підвищенню амплітуди дифракційних піків без помітної зміни їх положення, що свідчить про покращення кристалічності та розвиток текстури без фазових перетворень. Спектри комбінаційного розсіяння підтверджують ці результати. Вони демонструють поступову еволюцію структури від частково розупорядкованої у плівках після напилення до чітко виражених після термічної обробки коливальних мод, пов'язаних зі зв'язками Er–O, які також реєструються у спектрах ІЧ пропускання. Відсутність смуг поглинання, зумовлених нітратними групами, свідчить про повний розклад прекурсору при осадженні плівок. Отримані результати демонструють, що вибір прекурсору та способу нанесення плівок Er_2O_3 разом з орієнтацією підкладки та послідовними термічними обробками відіграють ключову роль у виготовленні хімічно чистих і структурно впорядкованих плівок Er_2O_3.

Ключові слова: Оксид ербію, Тонкі плівки, Дифракція рентгенівських променів, Інфрачервона спектроскопія, Комбінаційне розсіяння світла.